



26 **Abstract**

27 In mountain headwater streams the quality and resilience of cold-water habitat is regulated by
28 surface stream channel connectivity and groundwater exchange. These critical hydrologic
29 processes are thought to be influenced by the stream corridor bedrock contact depth (sediment
30 thickness), which is often inferred from sparse hillslope borehole information, piezometer
31 refusal, and remotely sensed data. To investigate how local bedrock depth might control summer
32 stream temperature and channel disconnection (dewatering) patterns, we measured stream
33 corridor bedrock depth by collecting and interpreting 191 passive seismic datasets along eight
34 headwater streams in Shenandoah National Park (Virginia USA). In addition, we used multiyear
35 stream temperature and streamflow records to calculate summer baseflow metrics along and
36 among the study streams. Finally, comprehensive visual surveys of stream channel dewatering
37 were conducted in 2016, 2019, and 2021 during summer baseflow conditions (124 total km of
38 stream length). We found that measured bedrock depths were not well-characterized by soils
39 maps or an existing global-scale geologic dataset, where the latter overpredicted measured
40 depths by 12.2 m (mean), or approximately four times the average bedrock depth of 2.9 m. Half
41 of the eight study stream corridors had an average bedrock depth of less than 2 m. Of the eight
42 study streams, Staunton River had the deepest average bedrock depth (3.4 m), the coldest
43 summer temperature profiles, and substantially higher summer baseflow indices compared to the
44 other study streams. Staunton River also exhibited paired air and water annual temperature signals
45 suggesting deeper groundwater influence, and the stream channel did not dewater in lower
46 sections during any baseflow survey. In contrast, streams Paine Run and Piney River did show
47 pronounced, patchy channel dewatering, with Paine Run having dozens of discrete dry channel
48 sections ranging 1 to greater than 300 m in length. Stream dewatering patterns were apparently



49 influenced by a combination of discrete deep bedrock (20 m+) features and more subtle sediment
50 thickness variation (1-4 m), depending on local stream valley hydrogeology. In combination
51 these unique datasets show the first large-scale empirical support for existing conceptual models
52 of headwater stream disconnection based on underflow capacity and shallow groundwater
53 supply.

54



55 **1. Introduction**

56 Mountain headwater stream habitat is influenced by hydrologic connectivity along the
57 surface channel, and connectivity between the channel and multiscale groundwater flowpaths
58 (Covino, 2017; Wohl, 2017). Discharge from shallow groundwater within the critical zone is a
59 primary component of stream baseflow, attenuating maximum summer temperatures and
60 creating cold water habitat (Singha and Navarre-Sitchler, 2021; Sullivan et al., 2021). In
61 headwater stream valleys characterized by irregular bedrock topography and thin, permeable
62 sediments, nested physical processes interact to control the connectivity of groundwater/surface
63 water exchange (Tonina and Buffington, 2009). Between stormflow and snowmelt events,
64 headwater streamflow (baseflow) is primarily generated by groundwater discharge due to a
65 relative lack of soil water storage and release (Winter et al., 1998). Unlike in lower valley
66 settings, mountain headwaters accumulate reduced fine soil, facilitating efficient routing of
67 quickflow to streams through macropores and other preferential flowpaths within regolith and
68 saprolite (Sidle et al., 2000). Recharge that does percolate vertically contributes to shallow
69 groundwater along steep hillslopes and valley floors, where groundwater flowpath depths are
70 constrained by bedrock topography (Buttle et al., 2004). Although deeper groundwater may also
71 represent an important contribution to summer streamflow in systems with relatively permeable
72 bedrock (Burns et al., 1998; O’Sullivan et al., 2020), shallow, low permeability bedrock
73 generally restricts stream-groundwater connectivity to the thin layers of unconsolidated
74 sediments (Briggs et al., 2018b).

75 In addition to baseflow drainage along headwater stream networks, down-valley shallow
76 groundwater ‘underflow’ can be substantial when high gradient streams lack sinuosity and flow
77 over permeable sediment (Figure 1a, Figure A1). In fact, headwater stream channels may only be
78 expected to show surface flow when the transmission ability of the underlying alluvium and

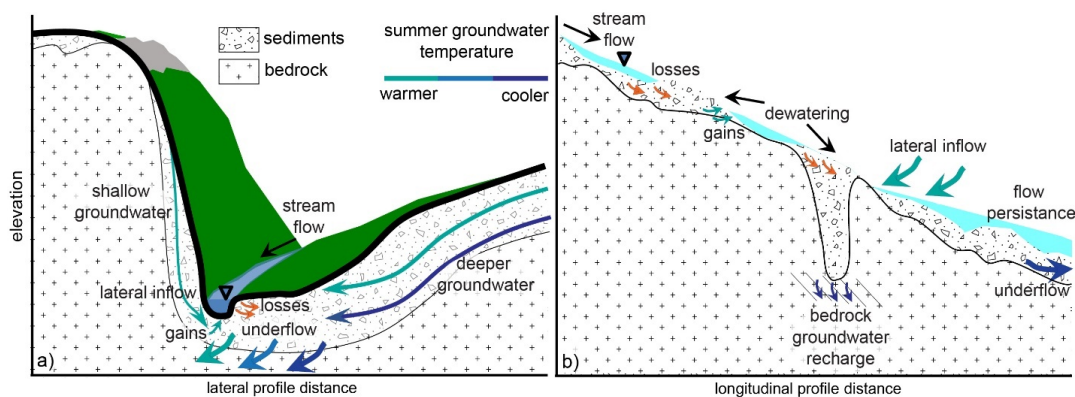


79 colluvium is exceeded, and bedrock depth is thought a primary control of this underflow capacity
80 (Ward et al., 2020). In some hydrogeologic settings, underflow can dominate groundwater export
81 from mountain catchments compared to groundwater drainage via the surficial stream channel
82 (Larkin and Sharp, 1992; Tiwari et al., 2017). Moreover, in addition to longitudinal transport
83 down-valley, underflow also acts as a reservoir of exchange for hyporheic flowpaths that may
84 mix with shallow groundwater before returning to channel flow (Payn et al., 2009), transporting
85 buffered temperature signals back to channel waters (Wu et al., 2020). Local underflow is
86 recharged from upgradient flowpaths and adjacent hillslopes, creating complex seasonal and
87 interannual patterns in groundwater connectivity and discharge to surface water (Jencso et al.,
88 2010; Johnson et al., 2017). A major challenge to understanding groundwater exchange in
89 headwaters is that attributes of the streambed subsurface, such as the depth to the underlying
90 bedrock contact, are often only available from limited direct measurements, coarse spatial
91 interpolations, or inferred remotely based on landscape forms. Therefore, methods that allow
92 efficient, local measurements of the streambed subsurface are critically needed.

93 Seasonal thermal regimes of mountain headwater streams can be profoundly impacted by
94 groundwater inflow from multiple depths (Briggs et al 2018a). In lower valley settings, the
95 temperature of groundwater discharge along stream networks is often assumed to approximate
96 the average annual land surface temperature throughout the year (Stonestrom and Constantz,
97 2003). Conversely, shallow groundwater temperature (within several m from land surface) can
98 show pronounced seasonality (Bundschuh, 1993; Lapham, 1989) and high spatial variability,
99 even over small spatial extents (Snyder et al. 2015). The warming of shallow groundwater during
100 the summer and fall seasons can limit the ability of gaining mountain streams to support cold-
101 water fish populations during the low flow season, even if baseflow (assumed to be dominated



102 by groundwater discharge) fractions are large (Johnson et al., 2020). In systems with low
103 permeability bedrock, thicker hillslope sediments may generate deeper, colder lateral
104 groundwater flow to streams in summer (Figure 1a), increasing cold water habitat resiliency
105 (Briggs et al., 2018b). For example, a recent meta-analysis of stream and air temperature records
106 across the contiguous United States found that a substantial fraction of shallow groundwater
107 dominated streams displayed summer warming trends in recent decades, while deeper
108 groundwater dominated streams were more stable (Hare et al., 2021). Steep mountain stream
109 systems such as those found in the Blue Ridge and Cascade mountains of the USA have been
110 found to show annual thermal regimes dominated by the annual thermal signals of shallow
111 groundwater (Johnson et al., 2020), indicating such streams may also be at risk for warming over
112 time, contrary to assumptions based on elevation alone.



114 *Figure 1. A conceptual mountain stream valley cross section (panel a) and longitudinal profile*
115 *(panel b) indicating the expected control of low permeability bedrock topography on*
116 *groundwater temperature, stream-groundwater exchange, patchy stream dewatering, and the*
117 *underflow reservoir.*

118 Beyond warm summer stream temperatures, the dewatering and disconnection of the
119 active stream channel during summer low flows can adversely impact fish habitat by impeding
120 fish movement (Edge et al., 2017; Labbe & Fausch, 2000; Rolls et al., 2012; Snyder et al.,
121 2013), locally degrading water quality (Hopper et al., 2020), and increasing predation risks in



122 isolated pools (Magoulick and Kobza 2003). However, the physical controls on localized stream
123 channel dewatering are not well characterized and likely involve a spectrum of nested gaining
124 and losing flowpaths. For mountain headwater streams, previous research has documented
125 general seasonal shifts in hydraulic gradients from gaining to losing, with closely coupled
126 streamflow and precipitation events, indicating a dominance of shallow routing rather than
127 deeper groundwater connectivity in maintaining streamflow (Zimmer and McGlynn, 2017).
128 Locally-losing sections of headwater stream channels can be associated with coarse, permeable
129 colluvial deposits from hillslope mass wasting processes (Costigan et al., 2016; Weekes et al.,
130 2015), as local enhancement of the total pore space under mountain streams can drive
131 downwelling of streamwater (Figure 1b, Tonina & Buffington, 2009). Main channel dewatering
132 occurs when the bed sediments have a storage and transport capacity that exceeds stream
133 discharge (Rolls et al., 2012; Ward et al., 2018), though stream water losses can also be driven
134 by local changes in bed morphology and slope (Costigan et al., 2016). The shallowing of the
135 underlying bedrock contact may drive lateral underflow toward the surface causing the channel
136 to gain water (Herzog et al., 2019)(Figure 1b), though such hypothesized dynamics are not well
137 documented in existing literature due to a relative lack of bedrock topography data along
138 headwater streams.

139 At large scales, contiguous bedrock depth layers are interpolated from a combination of
140 relatively sparse borehole data and surface topography (Kauffman et al., 2018; Pelletier et al.,
141 2016; Shangguan et al., 2017). However, in steep headwater systems with little borehole data,
142 bedrock topography is difficult to predict accurately from land surface topography alone. The
143 development of improved tools for predicting bedrock depth is an active area of research which
144 has recently demonstrated promise when bedrock outcrop data are included (e.g. Furze et al.,



145 2021; Odom et al., 2021). The limitations of using landform data to predict bedrock depth are
146 compounded by inherent challenges in collecting physical data via soil pits and monitoring wells
147 in rugged, rocky terrain, and so direct measurement data are often limited to highly studied
148 experimental watersheds where bedrock depth is inferred from piezometer installation refusal
149 (e.g. Jencso et al., 2010; Ward et al., 2018).

150 Application of near surface geophysical methods to stream corridor research has
151 increased appreciably in recent years (McLachlan et al., 2017), and several methods are sensitive
152 to shallow subsurface flow and geologic attributes including bedrock depth. Active seismic
153 refraction measurements can provide high resolution (10s of cm) bedrock depth information
154 along transect-based cross-sections (e.g. Flinchum et al., 2018), but are less suited for
155 exploration throughout rugged mountain stream valleys at the many km-scale due to logistical
156 challenges in using active seismic methods to obtain a sufficient amount of data to effectively
157 characterize important variation in bedrock depth at relatively small, ecologically-relevant spatial
158 scales. Point-based, efficient passive seismic measurements represent a unique combination of
159 high mobility and relative precision for measuring bedrock depth along mountain valleys. The
160 horizontal-to-vertical spectral ratio (HVSr) method is a passive seismic technique that evaluates
161 ambient seismic noise recorded using handheld instruments placed on the ground surface to
162 identify seismic resonance, which occurs at distinct unconsolidated sediment/bedrock interfaces
163 (Yanamaka et al., 1994).

164 The control of stream to groundwater exchange (i.e. ‘transmission losses’) on streamflow
165 permeance has been highlighted as an important research need by the comprehensive review of
166 intermittent stream systems by Costigan et al., (2016). Following the conceptual model of Ward
167 et al., (2018), a central hypothesis of our research was that bedrock depth along the stream



168 corridor will act as a first-order control on stream dewatering patterns when shallow bedrock is
169 of low permeability. Based on the concepts presented by Tonina & Buffington, (2009), we
170 postulated that relatively thick, permeable surficial sediment zones could locally accommodate
171 the entirety of low streamflow volumes, dewatering main channel sections at varied scales when
172 not balanced by groundwater inflow (Figure 1b). We further hypothesized that summer stream
173 channel thermal regimes would also be influenced by bedrock depth, as the temperature of
174 groundwater flowpaths that generate baseflow is depth dependent (Briggs et al., 2018b),
175 indicated conceptually in Figure 1a. To test our hypotheses, we extended the existing mountain
176 headwater bedrock depth surveys from Shenandoah National Park (SNP), Virginia, USA to
177 seven additional subwatersheds and compared results to physical mapping of stream dewatering,
178 multi-year stream temperature data and derived groundwater influence metrics, and baseflow
179 separation analysis to address the following research questions:

- 180 1. Does stream corridor bedrock depth exhibit longitudinal spatial structure in mountainous
181 streams? Can measured bedrock depth dynamics be accurately extracted from existing large-
182 scale datasets or inferred from high resolution soils maps?
- 183 2. Does underflow generally represent a net source or sink of summer flow for headwater
184 streams based on observed dewatering patterns and groundwater influence metrics?
- 185 3. Does bedrock depth explain spatial variation in stream temperature and summer baseflow
186 indices within headwater streams?

187 **2. Study Area**

188 The SNP is an 800 km² area of preserved headwater forest perched along a major
189 ridgeline of the Blue Ridge Mountains in northern VA, USA (Figure 2). The bedrock of the park
190 is predominantly low permeability basaltic and granitic material in the central and northern



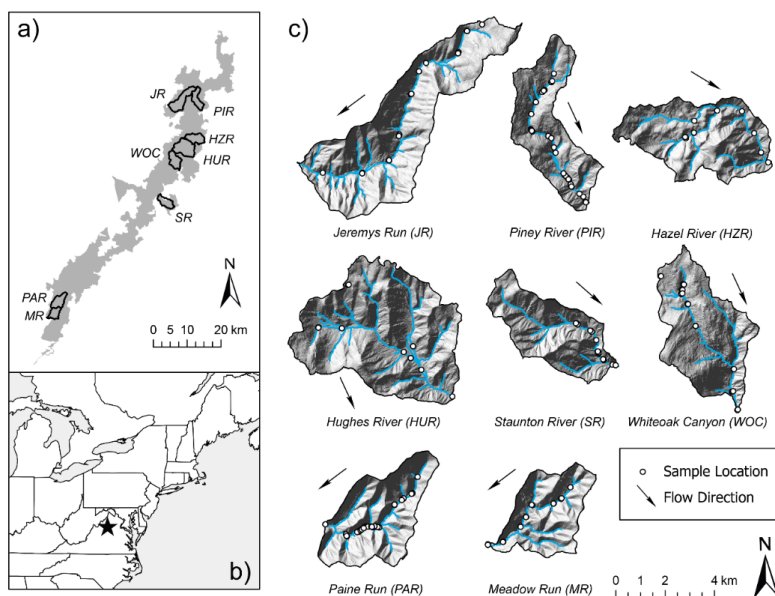
191 sections, and siliciclastic along the southern section (Southworth et al., 2009), though many
192 subwatersheds also transition in dominant bedrock type. Stream valleys of SNP are typically
193 steep and feature a perennial channel with mainly non-perennial tributaries (Johnson et al.,
194 2017), Figure A1) and stream baseflow consists of less than 3-yr old groundwater on average
195 (Plummer et al., 2001). In contrast, water collected from SNP hillslope wells completed in
196 shallow fractured rock generally have higher ages of 10-20 yr (Plummer et al., 2001), indicating
197 minimal contributions from bedrock groundwater to streamflow. Previous ecohydrological
198 research in SNP has noted that some mainstem stream channels show patchy dewatering at
199 summer low flows (Snyder et al., 2013), though the physical controls on these patterns of stream
200 drying were not clear.

201 In SNP, stream baseflow is thought to be predominantly generated by near-surface
202 drainage of coarse unconsolidated alluvium and colluvium (DeKay, 1972; Nelms and Moberg,
203 2010). The mountain ridgeline streamflow systems are expected to drain near-surface flowpaths
204 and accommodate substantial down valley underflow below perennial stream channels (Figure
205 A1). A portion of hillslope recharge is expected to percolate downward through connected
206 bedrock fractures into the deeper groundwater reservoir contributing to mountain block recharge
207 along the Shenandoah River Valley. Narrow alluvium deposits mapped along the stream
208 corridors of SNP are thought to generally range up to 6 m in thickness and be more clay rich
209 when sourced by basaltic bedrock (Southworth et al., 2009). Data at sparse wells drilled along
210 the SNP ridgeline indicate bedrock depth can range over 20 m on hillslopes and be highly
211 variable (DeKay, 1972; Goodling et al., 2020; Lynch, 1987).

212 Previous research has inferred summer and annual groundwater discharge patterns
213 throughout SNP subwatersheds based on paired, local air and stream water temperature



214 dynamics (Briggs et al., 2018a; Johnson et al., 2017; Snyder et al., 2015). Combined, these
215 analyses indicated groundwater exchange is highly variable in space along singular stream
216 valleys and between subwatersheds, and dependent upon local- to subwatershed-scale
217 characteristics. A combination of landform features that include stream slope and stream valley
218 confinement operate in conjunction with seasonal precipitation to drive groundwater influence
219 on summer stream temperatures (Johnson et al., 2017). Multi-week lags in time between
220 streamwater and local air annual temperature signals (i.e. phase shifts toward later time) were
221 observed from dozens of the 120 total monitored stream sites indicating a dominance of shallow
222 groundwater discharge, originating generally within approximately 3 m of land surface (Briggs
223 et al., 2018a).
224
225
226
227



229 *Figure 2. This study was based in Shenandoah National Park (panel a) located in the Blue Ridge*
230 *Mountains of northeast USA (panel b). LiDAR hillshade cutouts of each subwatershed illustrate*
231 *the rugged terrain and varied valley morphology (panel c). The mainstem stream channel and*
232 *tributaries are traced and HVSR measurement locations noted.*

233 3.0 Methods

234 3.1 Passive Seismic Bedrock Depth Measurements

235 Periodically from the summer of 2016 to the spring of 2020, we acquired 323 HVSR
236 measurements across SNP. The geophysical data were collected along the perennial streams of
237 seven subwatersheds with extensive existing stream temperature and ecological datasets, and at
238 known ridgeline and hillslope borehole locations. This effort added to previously interpreted
239 HVSR data from 22 riparian sites collected along the Whiteoak Canyon subwatershed in late
240 2015 (Briggs et al., 2017), for a total of 8 mountain streams for analysis in this study (Figure 2).

241 In July 2016, HVSR data were collected in the following subwatersheds: Piney River, Paine
242 Run, Meadow Run, Jeremy's Run, Hazel River, and Hughes River.



244 *Figure 3. Typical sections of a) Paine Run, b) Piney River, c) Staunton River, and d) a section of*
245 *Paine Run that was dewatered at baseflow leaving isolated pools. The passive seismic HVSR*
246 *instruments are shown deployed in panels a), b) and d) (Photographs by the U.S. Geological*
247 *Survey).*
248

249 Measurement locations mostly coincided with existing stream temperature monitoring
250 stations (described by Snyder et al., 2017), and were typically made at points immediately
251 adjacent to the stream or on larger rocks within the channel (Figure 3). In July 2019, HVSR data
252 were again collected along Paine Run and Piney River subwatersheds, and throughout the lower
253 Staunton River (Figure 3). The 2019 survey design differed in that transect measurements were
254 made at 4 locations along the stream channel waterline spaced approximately 25 m apart at
255 longitudinal locations that differed from the 2016 survey. This was done to assess potential
256 variation in bedrock depth along short subreaches of these three streams. Finally, clustered
257 HVSR data were collected in March 2020 in Paine Run and Piney River in zones previously



258 observed to show channel disconnection and streamflow re-emergence. Measurement locations
259 were chosen to test the hypothesis that the dewatering patterns were controlled by bedrock depth
260 as shown conceptually in Figure 1b.

261 HVSR data were collected using multi-component Tromino seismometers (MOHO,
262 S.R.L.) directly coupled to the land surface or placed on heavy metal plates where sediment was
263 loose. Collection times ranged 10-20 min at either 128 or 256 Hz sampling rates. HVSR data
264 collection locations were determined by a combination of internal Tromino GPS and external
265 GPS units. HVSR measurements were processed to derive a resonant frequency using a
266 commercially available program (GRILLA® v. 8.0 (2018); further details regarding data
267 processing are given by Goodling et al., (2020).

268 Resonant frequency measurements that passed a series of quality criteria were then
269 converted to a bedrock depth estimate following Briggs et al., (2017). This conversion
270 necessitates a shear wave velocity estimate for the unconsolidated sediments over bedrock.
271 HVSR data collected at spatially distributed boreholes with documented depth to varied-type
272 bedrock along the SNP ridgeline indicated a shear wave velocity of 358.7 +/- 56 m/s (Goodling
273 et al., 2020). A similar shear wave velocity of 346 m/s was measured at two locations along the
274 Whiteoak Canyon riparian zone spaced several km apart using active seismic methods (Briggs et
275 al., 2018b). This agreement indicates a common shear wave velocity can be assumed for the
276 unconsolidated material of SNP subwatersheds. For this study we used the average of these
277 spatially distributed active and passive seismic methods at 352 m/s. The mean shear wave
278 velocity calculated in this study is comparable to the mean shear wave velocity ranges in firm
279 soils (180 - 360 m/s) and very dense soil and soft rock (360-760 m/s), according to National
280 Earthquake Hazards Reduction Program (NEHRP) guidelines (Building Seismic Safety Council,



281 1994). As an example of measurement sensitivity to the shear wave velocity parameter for
282 shallow bedrock contacts, a velocity change in either direction by 25 m/s would generally shift
283 the bedrock depth estimate by <0.2 m.

284 *3.2 Observations of spatial dewatering patterns*

285 Longitudinal (upstream to downstream) patterns of dewatering were determined in the
286 summers of 2016, 2019, and 2021 during baseflow conditions over 124 total km of stream length
287 for all surveys combined. In July-August of 2016 all eight subwatersheds (Figure 2) were
288 surveyed. In September of 2019 and August 2021, dewatering surveys were repeated in three
289 subwatersheds (Paine Run, Piney River, and Staunton River) to evaluate annual variation in
290 dewatering patterns. Data were collected by team of investigators walking each stream from an
291 upstream location defined by the point along the stream draining 75-hectares (assumed capture
292 area required to generate perennial streamflow, determined using watershed tools in ArcGIS) to
293 the bottom of each watershed near the park boundary, and mapping transition points between
294 three hydrologic categories: Wet, dry, or isolated pools based upon investigator observation.
295 “Wet” segments were defined as reaches where entire channel was wet with flow between pools;
296 “Dry” segments were defined as reaches containing no water, or isolated pools of insufficient
297 depth to sustain 1+ year old brook trout; and “Isolated Pools” were defined as reaches containing
298 pools of sufficient depth to support brook trout but were hydrologically disconnected from other
299 parts of the channel. An example of isolated pools is photographically depicted in Figure 3d.
300 Spatial coordinates of transition points were mapped using a Trimble R2 GNSS receiver for <1 -
301 meter accuracy. Surveys for each subwatershed were completed within a single day to minimize
302 effects of temporal variation in precipitation.



303 In addition to local variability in bedrock depth, spatial patterns of dewatering and stream
304 temperature are likely to be influenced by seasonal precipitation and air temperature proximate
305 to the period of measurement (i.e., summer conditions, 2016 and 2019). We used historical
306 weather records (1942 – 2020) collected from the nearby Luray Weather Station located within
307 SNP (Station No. GHCND:USC00445096) to compare weather conditions during the two study
308 years with historical norms. Finally, 3D surface area of each subwatershed was determined from
309 existing LiDAR data using Add Surface Information in 3D Analyst Tools in ArcGIS and mean
310 valley width was evaluated from LiDAR data using 100-m transects measured approximately 2
311 m above the valley floor.

312 *3.3 Stream channel temperature data and baseflow separation*

313 Multi-year SNP stream temperature data were collected at hourly time intervals as
314 described by Snyder et al., (2017) using HOBO Pro V2 thermographs (+/- 0.2 °C expected
315 accuracy). From this larger dataset, 64 main channel locations within the 8 study subwatersheds
316 were extracted and processed for summary statistics such as the maximum and minimum of the
317 7-day running mean using Matlab R2019b software (Mathworks, Inc.). Only complete 7-day
318 periods were included in the running average. Warm season data (July, August, September) were
319 isolated and analyzed to coincide with the stream dewatering surveys and a larger body of
320 research regarding summer cold-water brook trout habitat in SNP. We utilized stream
321 temperature data processed by Briggs et al., (2018a) where dry sensor periods were identified
322 and removed, impacting a handful of the upper stream sites. Data were visualized and
323 downstream trends explored using Sigmaplot 14.0 software (Systat Software Inc.). Baseflow
324 separation was conducted for the three continuously gaged streams of this study (Paine Run,
325 Piney River, Staunton River) over summer months for the period of record (1993-2020).
326 Following the approach of (Hare et al., 2021), the daily Baseflow Index (BFI) was calculated



327 using the USGS-R ‘DVstats’ package (version 0.3.4) by dividing the calculated baseflow
328 discharge by the corresponding stream discharge, where a value of one would indicate stream
329 discharge was entirely composed of baseflow. BFI was then averaged (mean) across each
330 summer season, along with the mean and standard deviation of summer stream discharge.

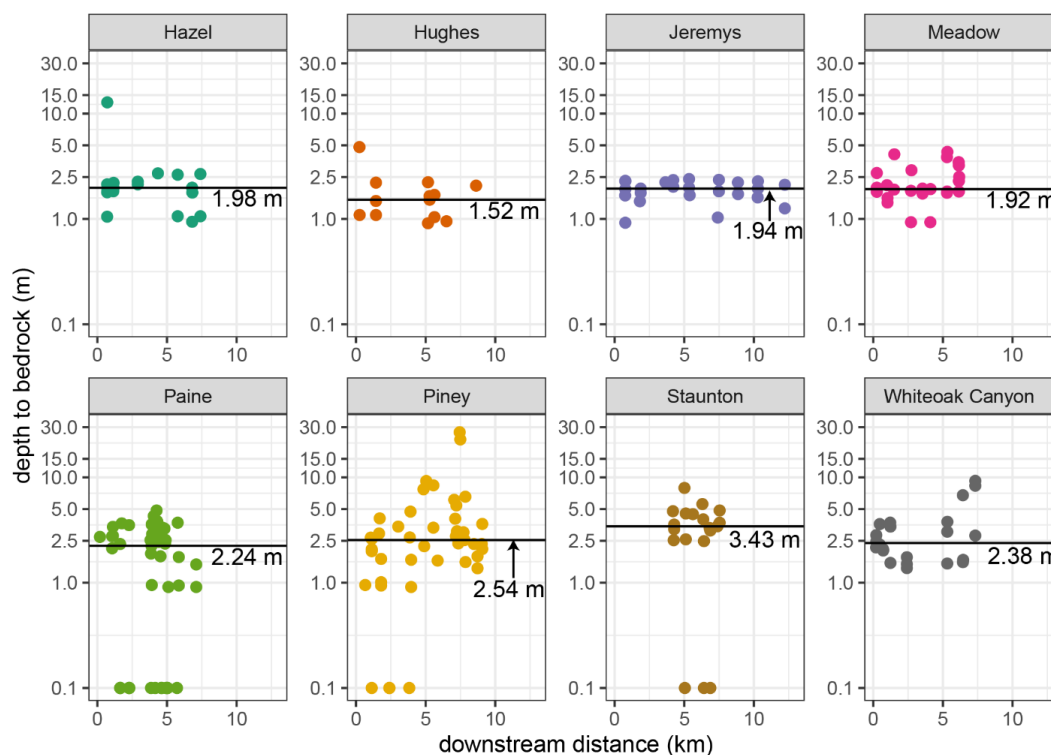
331 **4. Results**

332 *4.1 Stream Corridor Bedrock depth*

333 Approximately 60% of individual HVSR measurements (191 of the 323) were of high
334 enough quality to be interpreted for bedrock depth using objective data quality metrics reported
335 by the GRILLA software. This ratio of interpretable to total HVSR measurements was similar to
336 the previous 2015 Whiteoak Canyon Run study using the same instrument type (Briggs et al.,
337 2017). For the 132 datasets that could not be interpreted, the primary reason was no identifiably
338 resonant frequency ‘peak’ in the multicomponent seismic data, as described in more detail in the
339 data release of Goodling et al., (2020). The loosely consolidated, rocky surficial soils of many
340 SNP subwatershed riparian zones likely contributed to poor instrument coupling to the land
341 surface, and therefore reduced measurement sensitivity/success compared to firmer soils.
342 However, due to spatial redundancy in the measurements, the 191 locations where bedrock depth
343 was evaluated generally covered all the intended longitudinal stream measurement locations
344 throughout the subwatersheds.



345



347 *Figure 4. Measured depth to rock along the stream channel and riparian zones of the eight study*
348 *subwatersheds. Exposed bedrock (i.e., zero depth) observed at the intended measurement*
349 *location is noted here by a value of ‘0.1’ on the log scale. The median value is shown as a*
350 *labelled horizontal line.*

351

352 The median bedrock depth was smallest for Hughes River (1.52 m), and similar for
353 Meadow Run, Jeremy’s Run, Hazel River (1.92, 1.94, 1.98, respectively, Table 1, Table B1,
354 Figure 4). Paine Run had a median of 2.24 m, Whiteoak Canyon of 2.38 m, and Piney River of
355 2.54 m. Lower Staunton River had the largest median depth to rock of 3.43 m (Table 1). Piney
356 River had the largest variation in bedrock depth, including a discrete zone greater than 20 m
357 deep, along with several zones of exposed bedrock along the channel. Visual observations of



358 exposed channel bedrock were not incorporated into the bedrock depth averages presented in
 359 Table 1.

360 **Table 1.** *The median bedrock depth along with the elevation, mean, and 7-d maximum summer*
 361 *temperatures over the period of record collected at most downstream site location in each*
 362 *subwatershed.*

site	3D subwatershed surface area (km ²)	mean valley width (m)	median bedrock depth (m)	most downstream stream temperature site		
				elevation (m)	mean (°C)	7-d max (°C)
Hughes River	42.2	73.7	1.52	307	18.7	21.2
Meadow Run	15.0	55.3	1.93	450	18.4	20.4
Jeremy's Run	37.5	51.8	1.94	286	19.6	23.6
Hazel River	22.5	48.3	1.98	328	18.5	21.7
Paine Run	21.7	51.6	2.24	426	18.8	20.9
Whiteoak Cyn.	22.4	45.0	2.38	348	18.7	21.2
Piney River	20.6	48.6	2.54	371	17.9	20.6
Staunton River	18.0	45.6	3.43	309	17.4	19.9

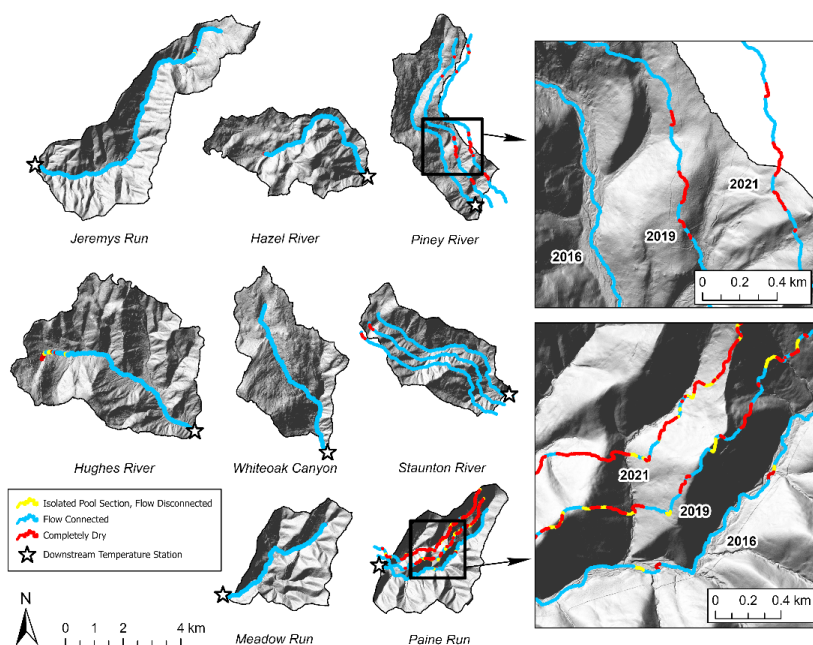
363

364 *4.2 Spatial Dewatering Patterns and Climate Data*

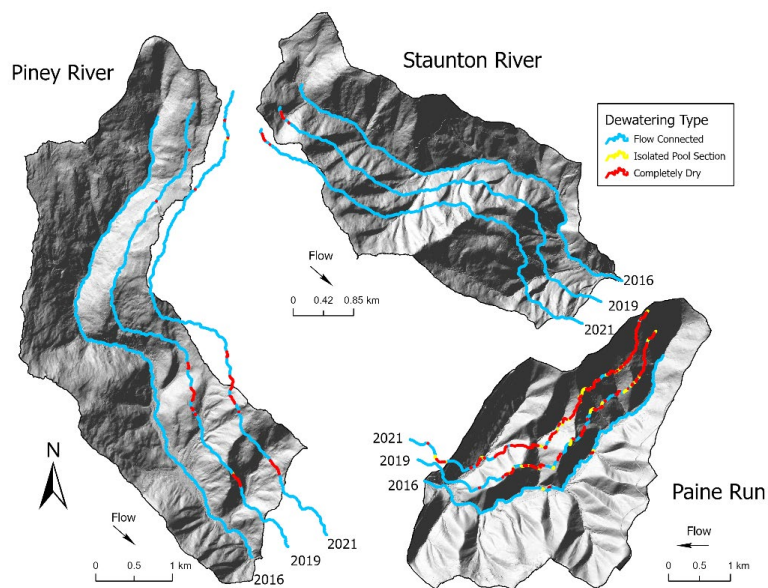
365 Cumulative monthly precipitation during baseflow summer (July-September) was higher
 366 than normal in 2016 and near average or lower than average (period of record 1942-2020),
 367 depending on the month, in 2019 (Figure A2). Mean monthly air temperatures were higher than
 368 average for both study years during baseflow summer reflecting the long-term trend of
 369 increasing air temperatures in the park (Luray weather station GHCND:USC00445096; see
 370 Menne et al. 2012). Patches of stream dewatering were observed along five of the eight study
 371 subwatersheds between 19-27 July, 2016, when over 98 km of total stream length were mapped
 372 (Figure 5). However, for Meadow Run, Hazel River, and Hughes River stream dewatering only
 373 occurred near the upper stream origination point. In contrast, Paine Run and Jeremy's Run had
 374 several discrete dewatering sections further from their origination points (examples shown in
 375 Figure 3d, Figure A3). During the drier period 17-19 September 2019, no dewatering was found
 376 along lower Staunton River, though Piney River had seven discrete dry patches where none were



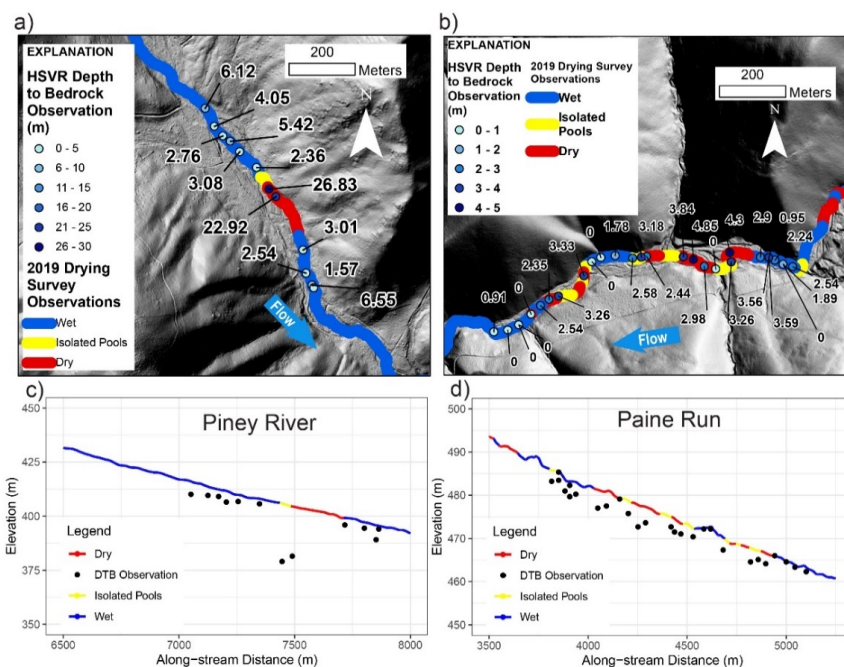
377 mapped in 2016, and similar patterns were observed for those two streams in 2021 (Figure 6).
378 Paine Run had 29 points of dewatering in 2019, distributed mainly along the central and upper
379 sections of the stream corridor, and showed extensive dewatering in 2021 (Figures 5, 6, 7). The
380 two Paine locations that were dry in 2016 were also dry in 2019 and 2021.



382 *Figure 5. Results from 2016, 2019, and 2021 longitudinal channel dewatering surveys conducted*
383 *by physical observation, where the 2019 and 2021 data are shown offset laterally from the*
384 *stream channel where those surveys occurred.*



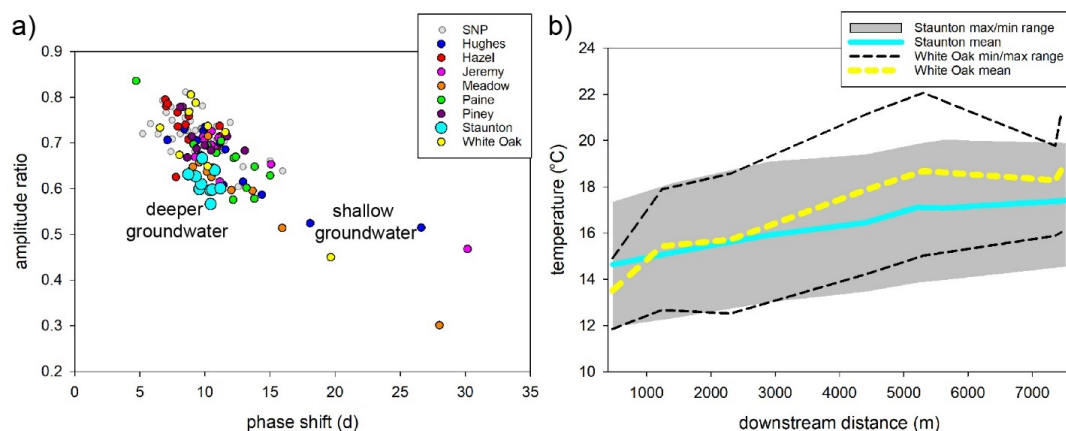
386 *Figure 6. Zoom views for the three subwatersheds where stream dewatering observations were*
387 *also collected in 2021.*
388
389
390



392 *Figure 7. The results of the 2019 stream drying survey and 2020 high spatial resolution HSVR*
 393 *measurements are shown over the LiDAR hillshade in plan view (panels a, b) and along a*
 394 *LiDAR-derived stream elevation profile cross-section view (panels c, d) for Piney River (panels*
 395 *a, c) and Paine Run (panels b, d).*

396 4.3 Stream Temperature Patterns

397 Paired air and water annual temperature signals exhibited a spectrum of shallow
 398 groundwater influences: phase shifts between stream and local air signals ranged from
 399 approximately 5 to 30 d with a mean of 11 d. Reduced annual temperature signal amplitude ratio
 400 generally corresponded with increased phase shift when all SNP stream monitoring sites are
 401 plotted in aggregate (Figure 8a). Staunton River stream sites cluster together and show less
 402 signal phase shift (mean of 10 d) for similar low amplitude ratio values (mean of 0.6) observed in
 403 other subwatersheds.

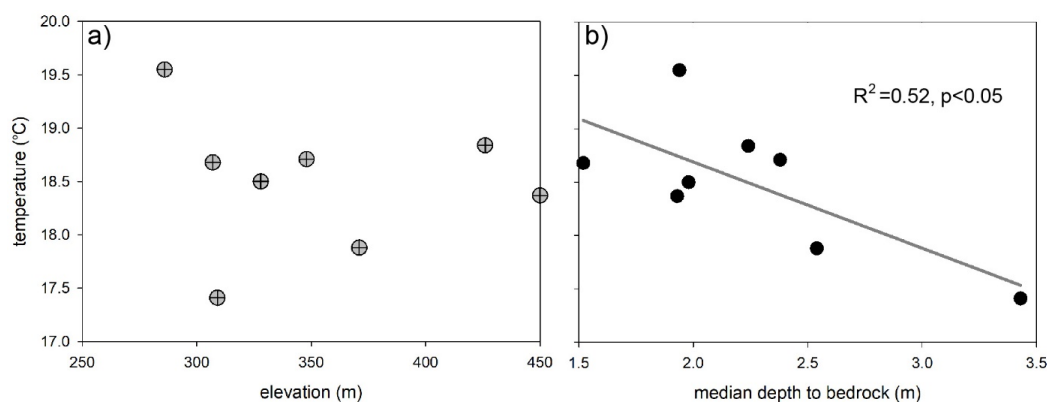


405 *Figure 8. Panel a) shows the annual temperature signal metrics for the study subwatersheds*
406 *highlighted within the larger SNP dataset with conceptual groundwater end member signature*
407 *trajectories. Panel b) displays the downstream mean summer temperature profiles and 7-d*
408 *maximum and minimum temperature ranges for Staunton River and Whiteoak Canyon.*

409
410 Although originating in a similar place, the downstream mean, 7-d maximum, and 7-d
411 minimum stream temperature profiles differed between Staunton River and Whiteoak Canyon,
412 where the latter had greater temperature variation and warming with downstream distance
413 (Figure 8b). The mean summer stream temperature had an approximate 2 °C total range over the
414 period of record. The warmest average (19.6 °C) and 7-d maximum (23.6 °C) was observed for
415 the lower Jeremy's Run site, which was also at the lowest elevation. However, only 23 m higher
416 in elevation, the downstream Staunton River site had the coldest average (17.4 °C) and 7-d
417 maximum (19.9 °C) summer temperature. Piney River, which has the second largest median
418 bedrock depth (2.54 m), had the second lowest average temperature (17.4 °C) at the lower site.
419 No significant relation was observed between elevation and mean summer temperature at the
420 lower stream monitoring site (Figure 9a), but a significant negative linear relation ($R^2=0.52$;
421 $p<0.05$) was determined between median stream corridor bedrock depth and mean summer
422 stream temperature (Figure 9b). However, there is strong leverage on the linear fit from the



423 Staunton River datapoint such that the Spearman rank test was not significant upon its removal
424 ($r=-0.42$; $p=0.29$).



426 *Figure 9. Mean summer temperature at the downstream monitoring site is shown plotted by a)*
427 *elevation, and b) median subwatershed bedrock depth. A significant linear relation was*
428 *determined with bedrock depth but not elevation.*

429 4.4 Baseflow Separation (Index)

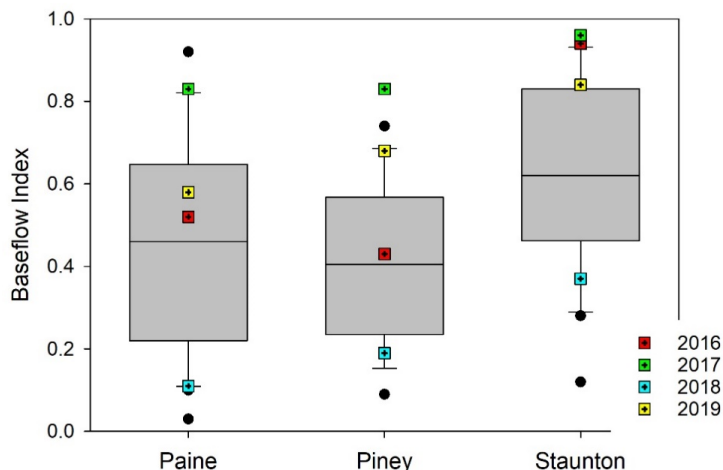
430 The summer season BFI determined for Paine Run, Piney River, and Staunton River over
431 show substantial variability, but the median summer BFI over the period of flow record for
432 Staunton River (0.62) is approximately 50% greater than Paine Run and Piney River (0.46 and
433 0.41, respectively, Table 2). For the primary study years of 2016-2019, Staunton River BFI is
434 always largest, and all sites are above their respective interquartile range in 2017 but below their
435 interquartile range in 2018 (Figure 10). The anomalously low 2018 BFI values can be explained
436 by extremely high summer precipitation that year (Figure S2), resulting in total streamflow being
437 dominated by runoff and quickflow as parsed with baseflow separation. Mean summer
438 streamflow over the period of record was highest for Piney River and lowest for Pain Run, and
439 overall summer streamflow was most stable for Staunton River (lowest coefficient of variation).

440 **Table 2.** The median summer Baseflow Index (BFI), mean summer streamflow, and mean summer
441 standard deviation (SD) streamflow for three gaged streams from 1993-2020.



<i>site</i>	<i>median BFI</i>	<i>mean streamflow (L/s)</i>	<i>mean coefficient of streamflow variation</i>
Paine Run	0.46	93.0	1.6
Piney River	0.41	164.4	1.7
Staunton River	0.62	157.3	0.7

442



444 *Figure 10. Summer Baseflow Index metrics summarized from 1993-2020 for three streams, with*
 445 *specific values from the primary study years identified.*

446 **5.0 Discussion**

447 *5.1 Longitudinal Spatial Structure in Observed Bedrock Depth*

448 Seminal groundwater/surface water exchange research has indicated that bedrock
 449 topography along headwater streams may be a first-order control on the arrangement of nested
 450 gaining and losing flowpaths (e.g. Tonina & Buffington, 2009), and increased (low permeability)
 451 bedrock depth is recognized as a primary driver of stream disconnection during dry periods that
 452 could be exacerbated by climate change (Ward et al 2020). However, despite the apparent
 453 importance to a range of headwater stream physical processes and cold-water habitat, local



454 bedrock depth data are almost universally lacking, even in heavily studied experimental
455 watersheds. Our study provides new inferences regarding the effects of bedrock depth on stream
456 flow continuity, groundwater exchange, and temperature patterns in mountain streams. The
457 combined datasets indicate stream channel bedrock depth assessments may be necessary to
458 support stream habitat assessments and predictions of stream connectivity under drought and
459 climate change when existing large-scale geologic datasets are not of sufficient spatial resolution
460 to support natural resource management applications.

461 Bedrock depth varied substantially within and among several of the eight study SNP
462 subwatersheds but was predominantly shallow. For half of the subwatersheds (Hughes River,
463 Meadow Run, Jeremy's Run, and Hazel River), median bedrock depth along the stream channel
464 and lateral riparian zone was less than 2 m and did not show notable variability with distance,
465 outside of one 12.8 m depth to rock location at upper Hazel River (Figure 4). This anomalous
466 measurement at Hazel was collected lateral to the stream on a valley terrace of colluvium, in the
467 vicinity of the only cold (approximately 10 °C at land surface) riparian spring that was observed
468 during all HVSR surveys. Bedrock depths of greater than 8 m were found along the upper
469 Whiteoak Canyon riparian zone as well (Briggs et al 2018a), also associated with surficial
470 seepage. Two anomalous bedrock depth measurements of 22.9 and 26.8 m were collected along
471 the Piney River channel, but instead of being associated with groundwater springs, they
472 coincided with a discrete sections of channel dewatering at baseflow during 2019 and 2021.
473 Therefore, it appears that discrete zones of thick surficial material are the exception along SNP
474 streams, though they can be important to localized processes such as focused riparian discharge
475 and streamflow disconnection (latter discussed in Section 5.2).



476 There are several existing sources of bedrock depth data that could potentially be used to
477 inform headwater stream modeling and habitat assessment, but the accuracy of such datasets
478 along headwater streams (typically away from existing boreholes) has generally not been
479 evaluated. We conducted a point-scale comparison of our relatively high-resolution bedrock
480 depth measurements to the global bedrock depth map of Shangguan et al., (2017) and found that
481 bedrock depths were almost universally overpredicted at the SNP by large margins (Figure A4).
482 Specifically, predictions from the global-scale dataset exceeded HSVR measured depths by
483 +12.2 m (mean), or approximately four times the average bedrock depth (2.9 m). As baseflow
484 generation is expected to be dominated by shallow groundwater sourced from unconsolidated
485 sediment in these headwater systems, this differential could propagate substantial uncertainty
486 into process-based groundwater flow model predictions if the global-scale dataset was used to
487 inform model structure.

488 Publicly available maps of surficial geologic materials are another potential source of
489 bedrock depth information. High-resolution digital soils maps are now widely available,
490 including for the catchments of SNP, and these maps do capture some of the general depth to
491 rock transitions between subwatersheds observed in this study. For example, NRCS (2020)
492 (<https://websoilsurvey.sc.egov.usda.gov/App/WebSoilSurvey.aspx>, accessed 12/10/2020)
493 indicate that the Whiteoak Canyon stream corridor is comprised of silts, loams, and stony soils
494 with a general bedrock depth of approximately 1.2 m., which is in a similar range as most HSVR
495 measurements made along the upper stream section (Figure 4). However, the generalized soil
496 units may not offer needed detail regarding site-specific valley sediment thickness for
497 hydrogeological and ecological studies where information regarding within-watershed variation
498 is critical. Along lower Piney River, where HSVR data had depths to rock ranging 1.4 to 3.6 m,



499 the NRCS soils map universally indicates silt and stony material > 2 m. Along Paine Run, where
500 the stream is often scoured to bedrock, the soils map shows consistent highly permeable sandy
501 material with > 2 m thickness. This discrepancy is understandable given most of the test pits
502 were likely substantially further downstream in better terrain for agriculture. In conclusion,
503 analysis of large-scale patterns from existing soils maps and interpolated/predicted bedrock
504 depth layers indicates that more precise geophysical mapping of bedrock depth may be needed to
505 inform stream research and management, particularly in shallow, low-permeability bedrock
506 terrain.

507 *5.2 Summer Stream Dewatering Related to Bedrock depth*

508 Aligned with the conceptual model of Ward et al., (2018), our central hypothesis was
509 bedrock depth along the stream corridor acts as a primary control on longitudinal stream
510 dewatering and flow disconnection during summer low flows (visual example shown in Figure
511 A3). We postulated that permeable streambed thickness may undulate along mountain stream
512 channels, and relatively thick sub-stream sediment zones could accommodate the entirety of low
513 streamflow volumes, locally disconnecting channels during seasonal drydown. We found mixed
514 support for this simple hypothesis. Hazel River and Hughes River were two of the three
515 subwatersheds that had dry channel zones just downstream of their respective stream origination
516 points in 2016, and these two riparian corridors also had their deepest riparian bedrock depths in
517 those high-elevation areas. However, as discussed above, Whiteoak Canyon had relatively thick,
518 porous sediment zone near the subwatershed outlet but did not show any zones of dewatering,
519 nor did lower Staunton River in 2016, 2019, or 2021, despite having the deepest median bedrock
520 contact. Jeremy's Run had three mapped dry zones in 2016 (not surveyed in 2019), yet depth to
521 rock in those areas was only approximately 2 m, though the HVSR data collection points were
522 not perfectly aligned with the dry patches. To address this spatial mismatch in stream dewatering



523 and HVSR data, we used the stream dewatering maps to guide two new high-resolution HVSR
524 surveys in March 2020 along sections of Paine Run and Piney River with dynamic patterns of
525 channel drying, as described below.

526 When bedrock depth data were collected at high-resolution, even more variability in
527 bedrock topography/sediment thickness was revealed than in the original larger-scale surveys,
528 and that finer scale of information was relevant to understanding stream dewatering patterns.
529 For example, during summer 2019, a 291 m length section of lower Piney River was observed to
530 be dry, and immediately preceded by 62 m of isolated stream channel pools, and a nearly
531 identical dewatering pattern was observed there in 2021 (Figures 6,7a,c). The upper portion of
532 this major feature of stream disconnection corresponded directly with a transition in bedrock
533 depth along the channel from approximately 3 m to adjacent measurements of 27 and 23 m. This
534 ‘trough’ in the bedrock surface can likely act as a streamwater sink (shown conceptually in
535 Figure 1b), routing surface water downward to the point of draining the channel locally in the
536 summers of 2019 and 2021, but not in 2016 when precipitation (groundwater supply) was higher
537 than normal. Further downstream, the bedrock depth returned to approximately 3 m near the
538 furthest downstream measurement point, and flowing channel water was again noted during the
539 drying surveys. Such a section of stream dewatering in the lower watershed would serve to
540 impede fish passage along Piney River during the lowest flows, likely corresponding to times of
541 maximum thermal stress when fish mobility is critical to seeking thermal refuge (Magoulick and
542 Kobza, 2003).

543 Not all variability in bedrock depth below streams associated with stream drying was as
544 dramatic as the Piney River example but can be important in disconnecting channel habitat in
545 summer. Paine Run is a more strongly confined stream valley that had 29 discrete zones of



546 stream channel dewatering during September of 2019 and extensive dewatering in 2021, when
547 numerous dead brook trout were also noted (Figures 5,6,7b,d). Paine also had the greatest total
548 exposed bedrock out of any of the SNP subwatersheds in this study, indicating a highly
549 constrained valley underflow reservoir. High resolution bedrock depth data was collected over a
550 Paine Run subreach with seven discrete dry patches ranging from 17 m to 185 m in channel
551 length, with many bordered by zones of isolated pools (Figure 7b). A comparison of these
552 patterns with bedrock depth along the channel shows the flowing sections of stream were
553 dominated by exposed bedrock surfaces or thin sediment. However, a notable exception is
554 toward the upstream end of this focus reach, where depth to rock was consistently > 2 m over the
555 run up to a large zone of disconnected channel with some isolated pools (Figure 7b,d). This
556 result suggests the losses of stream water accumulated over this approximately 80 m channel
557 distance. In the following downstream contiguous sections of dry channel and/or isolated pools,
558 bedrock depth averaged a larger 3.3 m, indicating the entirety of streamflow was accommodated
559 by the subsurface, congruent with our original hypothesis. However, knowledge of bedrock
560 depth in isolation is clearly not sufficient to predict stream channel gaining, losing, and
561 disconnection patterns as the stream with the largest average bedrock depth, lower Staunton
562 River (median depth to rock 3.4 m, Figure 4), was not observed to dewater during any of the
563 three physical surveys (Figures 5,6).

564 *5.3 Summer Stream Temperature and Groundwater Exchange Dynamics*

565 Although headwater stream heat budgets are complex, our data indicates groundwater
566 connectivity plays an important role when stream temperatures are already close to aquatic
567 species thermal tolerances. The apparent dominance of shallow (< 3 m depth) groundwater
568 discharge along Whiteoak Canyon contributed to the Briggs et al. (2018b) prediction that the
569 lower reaches would not provide suitable brook trout habitat by the end of the century given



570 anticipated atmospheric warming. Jeremy's Run, a long (13.4 km) stream consistently underlain
571 by a shallow bedrock contact (median depth < 2 m), already shows a 7-d maximum summer
572 temperature that exceeds expected brook trout tolerances (i.e., >23.3 °C mean weekly average
573 temperature, Wehrly et al., (2007)) along the lowest reach.

574 The underflow reservoir of headwater stream valleys integrates upgradient and lateral
575 hillslope groundwater flowpaths, which accumulate with distance when bounded by low
576 permeability bedrock. The two subwatersheds with largest median bedrock depth along their
577 respective upstream corridors had the coldest mean summer temperatures, with Staunton River
578 standing out as distinctly colder, and having the only 7-d max temperature below 20 °C (Table
579 1). There was a significant relation between median bedrock depth and mean summer stream
580 temperature at the lower stream sites but not with elevation (Figure 9), indicating exchange with
581 groundwater had disrupted the expected elevation control on lower reach cold water habitat.
582 Surficial hillslope contributing area is often assumed a primary control on potential groundwater
583 discharge at the stream subreach scale. However, Staunton River also had the second smallest
584 drainage surface area of all study subwatersheds, and it is often assumed that lateral groundwater
585 inflow to headwater streams is related to presumed upslope contributing area. Further, Staunton
586 River did not have an average valley bottom width that was greater than other streams that were
587 observed to dewater.

588 Our research indicates that the vertical shallow aquifer dimension, as represented by
589 bedrock depth, is likely an important control of groundwater storage and connectivity to the
590 stream corridor. This conclusion is supported by the paired air/water annual temperature signal
591 metrics, indicating Staunton River sites cluster in the stronger, deeper groundwater influence
592 compared to most observations along the other SNP streams (Figure 8a). Therefore, it seems



593 there are important tradeoffs between bedrock depth along the stream channel as a driver of
594 stream dewatering and sediment thickness along the valley floor and hillslopes as a potential
595 source of stream baseflow.

596 For a more in-depth analysis the paired bedrock depth and groundwater inflow controls
597 on headwater summer stream dynamics, Staunton River can be contrasted with Paine Run. The
598 latter had a similar drainage surface area to Staunton River, but a 1.2 m shallower bedrock depth
599 on average, showed dozens of dewatered stream channel sections in 2019 and 2021, and had a
600 downstream boundary summer stream temperature that was 1.4 °C warmer. In addition to a
601 reduced average bedrock depth, Paine Run had numerous sections of exposed bedrock adjacent
602 to localized pockets of stream channel alluvium and colluvium (Figure 4, 7), while extensive
603 colluvial deposits along the Staunton River channel limited exposed bedrock to a few m-scale
604 sections associated with pool steps (Figure 4). Lower Staunton experienced major debris flows in
605 June, 1995 (Morgan and Wieczorek, 1996), events that likely created an enhanced local
606 groundwater reservoir within coarse hillslope material compared to other SNP subwatersheds.

607 Based on the integrated datasets from these two SNP streams, we conclude that
608 groundwater exchange is a critical factor determining whether headwater streams will warm and
609 dewater in summer, which in turn is controlled in part by the thickness of supra-bedrock
610 unconsolidated aquifer. As noted above, annual temperature metrics indicated a consistently
611 deeper groundwater discharge influence along Staunton River, while Paine Run had annual
612 signal metrics that mainly indicated reduced and/or more shallow groundwater influence (Figure
613 9a). Long term streamflow and baseflow analysis from these streams showed Staunton River had
614 higher, but more stable summer discharge (Table 1), and substantially higher median summer
615 BFI (0.62 vs 0.46), indicating greater dominance of groundwater as a generator of streamflow

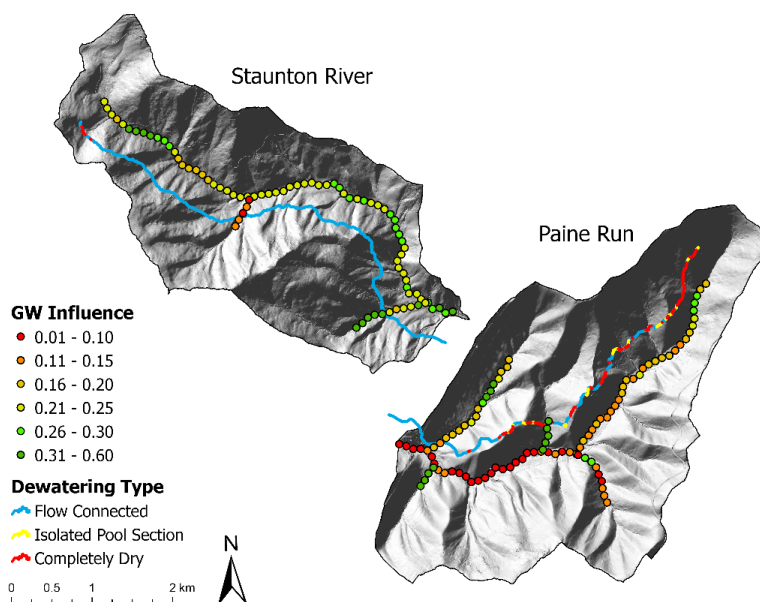


616 compared to runoff and quickflow. Previous research in SNP used paired air/stream water
617 temperature records, precipitation, and landscape characteristics to statistically model
618 ‘groundwater influence’ by year on a scale of 0-1 at the 100-m scale along the streams of this
619 study, where details are described by Johnson et al., (2017). Although this previous work only
620 extended to 2015, that year had analogous BFI scores to 2019 for Staunton River (0.88 vs 0.84)
621 and Paine Run (0.60 vs 0.58). Comparing the 2019 drying survey observations to the 2015 high
622 spatial resolution modeling of groundwater influence we found that Paine Run was predicted to
623 have groundwater influenced tributaries, but along the mainstem, where extensive dewatering
624 was observed, there was substantially reduced modeled groundwater influence compared to the
625 mainstem of Staunton River (Figure 11).

626

627

628



630 *Figure 11. The 2019 stream dewatering survey data (lines; this study), plotted offset of the*
631 *mainstem, and 100-m groundwater influence predictions (points from Johnson et al., 2017),*
632 *plotted along the mainstem and tributaries, of Staunton River and Paine Run.*
633 *This observation and model comparison represents another line of evidence that groundwater*
634 *connectivity at the sub-reach scale is key in determining whether local increases in depth to*
635 *bedrock drive channel dewatering at low flow. The impact of reduced underflow groundwater*
636 *supply on stream disconnection is likely exasperated by the extensive zones of exposed bedrock*
637 *along Paine Run (Figure 4, 7d), which locally reduce groundwater mounding in stream valley*
638 *sediments as shown conceptually in Figure 1b, such that abrupt increases in bedrock depth cause*
639 *stream dewatering. Among the eight streams investigated here, Staunton River likely represents*
640 *the most resilient summer cold water habitat, which could not be predicted using bedrock depth*
641 *data alone but necessitated paired assessment of groundwater discharge dynamics.*



642 **6 Conclusions**

643 In steep mountain valley stream systems underlain by low-permeability bedrock, the
644 longitudinal underflow reservoir serves as a complex mechanism of streamflow generation,
645 streamflow losses, and stream temperature control (Figure 1, Supplementary Figure S1). Our
646 study utilized complimentary geophysical, temperature, and hydrologic data at the scale of eight
647 subwatersheds to highlight apparent tradeoffs in bedrock depth, shallow groundwater supply, and
648 the quality of cold-water habitat. Certain mountain stream corridor parameters may be
649 reasonable to assume or infer from high-resolution topographic data, such surficial sediment
650 permeability (based on land surface roughness) and stream valley width, which are primary
651 controls on whether underflow serves as a net source or sink of stream water (Flinchum et al.,
652 2018; Ward et al., 2018). However, as shown here, advances in predicting hydrologic
653 connectivity and thermal variation along mountain stream networks may also require local
654 evaluation of bedrock depth and stream-groundwater exchange.

655 When local increases in bedrock depth are not balanced by groundwater inflow, streams
656 may be expected to dewater and disconnect under low flow conditions, and streams with reduced
657 deeper groundwater influence show warmer summer temperatures. Contrary to what might be
658 expected, we found that mean summer stream temperature at was not significantly related to
659 elevation at all lower study boundaries, but instead was (negatively) related to average stream
660 bedrock depth. Staunton River had the coldest summer stream temperatures and most
661 pronounced deeper groundwater signatures. However, that subwatershed was of relatively small
662 total surface area and average valley width. The defining physical feature of Staunton River was
663 that it had the largest average bedrock depth of all the eight SNP study streams at 3.4 m,
664 allowing greater overall storage of recharge and baseflow generation. The other two gaged



665 streams had substantially reduced baseflow indices, indicating streamflow generation was
666 dominated by runoff and quickflow.

667 Overall, SNP streams tended to have consistently shallow bedrock depth, though a subset
668 were more variable or had spatial trends and discrete features. Observed channel dewatering
669 patterns during late summer baseflow periods were related to local scale variation in bedrock
670 depth, such as a discrete feature of greater than 20 m depth observed along Piney River that
671 caused repeated streamflow disconnection. However, in other streams more subtle bedrock depth
672 variation also caused channel dewatering, indicating the importance of local hydrogeological
673 context in determining the importance of bedrock depth on streamflow connectivity. For
674 example, patchy 2-4 m deposits of sediment adjacent to exposed bedrock along Paine Run
675 caused extensive summer dewatering in 2019 and 2021, and during the latter survey many dead
676 brook trout were noted in the disconnected sections. Paine and Piney also showed enhanced
677 dewatering during the summers of 2019 and 2021 compared to the wetter 2016 summer,
678 demonstrating the additional control of recent precipitation on stream disconnection in headwater
679 systems that do not efficiently store water.

680 Lateral groundwater inflow through high permeability, unconsolidated sediments is a
681 critical component of headwater stream baseflow (Tran et al., 2020). Shallow, low permeability
682 bedrock can constrain lateral flowpaths and underflow to the near surface critical zone, where it
683 is highly sensitive to enhanced evapotranspiration, temperature increase, and drought under
684 climate change (Condon et al., 2020; Hare et al., 2021). As it becomes increasingly important to
685 understand and predict the resilience of mountain cold-water stream habitat at a fine spatial
686 grain, continued coupled advances in geophysical characterization, stream temperature
687 monitoring, and groundwater exchange analysis are needed.



688 **Data Availability**

689 The data described in this manuscript are available at: doi.org/10.5066/F7B56H72,
690 doi.org/10.5066/F7JW8C04, and doi.org/10.5066/P9IJMGIB

691 **Author contribution**

692 *Conceptualization*: M.A. Briggs, Z.C. Johnson, C.D. Snyder, N.P. Hitt; *Investigation*: M.A.
693 Briggs, P. Goodling, Z.C. Johnson, C.D. Snyder, K.M. Rogers, N.P. Hitt; *Visualization*: M.A.
694 Briggs, K.M. Rogers, P. Goodling, J.B. Fair, C.D. Snyder. All authors contributed to the formal
695 analysis varied stages of writing.

696 **Competing interests**

697 The authors declare that they have no conflict of interest.

698 **Acknowledgments**

699 The authors gratefully acknowledge support from Natural Resource Preservation Program and
700 the U.S. Geological Survey (USGS) Chesapeake Bay Priority Ecosystems Science and Fisheries
701 Program. We also thank the Shenandoah National Park Staff for site access and general support
702 and field support from John Lane, David Nelms, Adam Haynes, Erin Snook, David Weller, Evan
703 Rodway, Jacob Roach, Matt Marshall, Joe Dehnert, and Mary Mandt. Any use of trade, firm, or
704 product names is for descriptive purposes only and does not imply endorsement by the U.S.
705 Government.

706



707 References

- 708 Briggs, M.A., Johnson, Z.C., Snyder, C.D., Hitt, N.P., Kurylyk, B.L., Lautz, L., Irvine, D.J.,
709 Hurley, S.T., Lane, J.W., 2018a. Inferring watershed hydraulics and cold-water habitat
710 persistence using multi-year air and stream temperature signals. *Sci. Total Environ.* 636.
711 <https://doi.org/10.1016/j.scitotenv.2018.04.344>
- 712 Briggs, M.A., Lane, J.W., Snyder, C.D., White, E.A., Johnson, Z.C., Nelms, D.L., Hitt, N.P.,
713 2018b. Shallow bedrock limits groundwater seepage-based headwater climate refugia.
714 *Limnologia* 68, 142–156. <https://doi.org/10.1016/j.limno.2017.02.005>
- 715 Briggs, M.A., Lane, J.W., Snyder, C.D., White, E.A., Johnson, Z.C., Nelms, D.L., Hitt, N.P.,
716 2017. Seismic data for study of shallow mountain bedrock limits seepage-based headwater
717 climate refugia, Shenandoah National Park, Virginia: U.S. Geological Survey data release.
718 <https://doi.org/10.5066/F7JW8C04>
- 719 Bundschuh, J., 1993. Modeling annual variations of spring and groundwater temperatures
720 associated with shallow aquifer systems Computer model. *J. Hydraul. Eng.* 142, 427–444.
- 721 Burns, D.A., Murdoch, P.S., Lawrence, G.B., Michel, R.L., 1998. Effect of groundwater springs
722 on NO₃⁻ concentrations during summer in Catskill Mountain streams. *Water Resour. Res.*
723 34, 1987–1996. [https://doi.org/Cited By \(since 1996\) 98Export Date 4 April 2012](https://doi.org/Cited%20By%20(since%201996)%2098Export%20Date%204%20April%202012)
- 724 Condon, L.E., Atchley, A.L., Maxwell, R.M., 2020. Evapotranspiration depletes groundwater
725 under warming over the contiguous United States. *Nat. Commun.* 11.
726 <https://doi.org/10.1038/s41467-020-14688-0>
- 727 Costigan, K.H., Jaeger, K.L., Goss, C.W., Fritz, K.M., Goebel, P.C., 2016. Understanding
728 controls on flow permanence in intermittent rivers to aid ecological research: integrating
729 meteorology, geology and land cover. *Ecohydrology* 9, 1141–1153.
730 <https://doi.org/10.1002/eco.1712>
- 731 Covino, T., 2017. Hydrologic connectivity as a framework for understanding biogeochemical
732 flux through watersheds and along fluvial networks. *Geomorphology* 277, 133–144.
733 <https://doi.org/10.1016/j.geomorph.2016.09.030>
- 734 DeKay, R.H., 1972. Development of ground-water supplies in Shenandoah National Park,
735 Virginia. *Virginia Div. Miner. Resour. Rep.* 10, 158.
- 736 Edge, C.B., Fortin, M.J., Jackson, D.A., Lawrie, D., Stanfield, L., Shrestha, N., 2017. Habitat
737 alteration and habitat fragmentation differentially affect beta diversity of stream fish
738 communities. *Landsc. Ecol.* 32, 647–662. <https://doi.org/10.1007/s10980-016-0472-9>
- 739 Flinchum, B.A., Holbrook, W.S., Grana, D., Parsekian, A.D., Carr, B.J., Hayes, J.L., Jiao, J.,
740 2018. Estimating the water holding capacity of the critical zone using near-surface
741 geophysics. *Hydrol. Process.* 32, 3308–3326. <https://doi.org/10.1002/hyp.13260>
- 742 Furze, S., Sullivan, A.M.O., Allard, S., Pronk, T., Curry, R.A., 2021. A High-Resolution ,
743 Random Forest Approach to Mapping Depth-to-Bedrock across Shallow Overburden and
744 Post-Glacial Terrain 1–23.
- 745 Goodling, P.J., Briggs, M.A., White, E.A., Johnson, Z.C., Haynes, A.B., Nelms, D.L., Lane,



- 746 J.W., 2020. Passive seismic data collected along headwater stream corridors in Shenandoah
747 National Park in 2016 - 2020: US Geol. Surv. Data Release.
748 <https://doi.org/doi.org/10.5066/P9IJMGIB>
- 749 Hare, D.K., Helton, A.M., Johnson, Z.C., Lane, J.W., Briggs, M.A., 2021. Continental-scale
750 analysis of shallow and deep groundwater contributions to streams. *Nat. Commun.* 1–10.
751 <https://doi.org/10.1038/s41467-021-21651-0>
- 752 Herzog, S.P., Ward, A.S., Wondzell, S.M., 2019. Multiscale Feature-feature Interactions Control
753 Patterns of Hyporheic Exchange in a Simulated Headwater Mountain Stream. *Water*
754 *Resour. Res.* 55, 10976–10992. <https://doi.org/10.1029/2019WR025763>
- 755 Hopper, G.W., Gido, K.B., Pennock, C.A., Hedden, S.C., Frenette, B.D., Barts, N., Hedden,
756 C.K., Bruckerhoff, L.A., 2020. Nowhere to swim: interspecific responses of prairie stream
757 fishes in isolated pools during severe drought. *Aquat. Sci.* 82, 1–15.
758 <https://doi.org/10.1007/s00027-020-0716-2>
- 759 Jencso, K.G., McGlynn, B.L., Gooseff, M.N., Bencala, K.E., Wondzell, S.M., 2010. Hillslope
760 hydrologic connectivity controls riparian groundwater turnover: Implications of catchment
761 structure for riparian buffering and stream water sources. *Water Resour. Res.* 46, 1–18.
762 <https://doi.org/10.1029/2009WR008818>
- 763 Johnson, Z.C., Johnson, B.G., Briggs, M.A., Devine, W.D., Snyder, C.D., Hitt, N.P., Hare, D.K.,
764 Minkova, T. V., 2020. Paired air-water annual temperature patterns reveal hydrogeological
765 controls on stream thermal regimes at watershed to continental scales. *J. Hydrol.* 587,
766 124929. <https://doi.org/10.1016/j.jhydrol.2020.124929>
- 767 Johnson, Z.C., Snyder, C.D., Hitt, N.P., 2017. Landform features and seasonal precipitation
768 predict shallow groundwater influence on temperature in headwater streams. *Water Resour.*
769 *Res.* 53, 5788–5812. <https://doi.org/10.1002/2017WR020455>
- 770 Kauffman, L.J., Yager, R.M., Reddy, J.E., 2018. Sediment and Aquifer Characteristics of
771 Quaternary Sediments in the Glaciated Conterminous United States: U.S. Geol. Surv. data
772 release. <https://doi.org/10.5066/F7HH6J8X>
- 773 Labbe, T.R., Fausch, K.D., 2000. Dynamics of intermittent stream habitat regulate persistence of
774 a threatened fish at multiple scales. *Ecol. Appl.* 10, 1774–1791.
775 <https://doi.org/10.1890/1051-0761>
- 776 Lapham, W.W., 1989. Use of temperature profiles beneath streams to determine rates of vertical
777 ground-water flow and vertical hydraulic conductivity. *US Geol. Surv. Water-Supply Pap.*
778 2337.
- 779 Larkin, R.G., Sharp, J.M., 1992. On the relationship between river-basin geomorphology, aquifer
780 hydraulics, and ground-water flow direction in alluvial aquifers. *Geol. Soc. Am. Bull.* 104,
781 1608–1620.
- 782 Lynch, D.D., 1987. Hydrologic conditions and trends in Shenandoah National Park, Virginia,
783 1983–84. *Water- Resour. Investig. Rep.* 87–4131.
- 784 Magoulick, D.D., Kobza, R.M., 2003. The role of refugia for fishes during drought: A review
785 and synthesis. *Freshw. Biol.* 48, 1186–1198. <https://doi.org/10.1046/j.1365->



- 786 2427.2003.01089.x
- 787 McLachlan, P.J., Chambers, J.E., Uhlemann, S.S., Binley, A., 2017. Geophysical
788 characterisation of the groundwater–surface water interface. *Adv. Water Resour.* 109, 302–
789 319. <https://doi.org/10.1016/j.advwatres.2017.09.016>
- 790 Meisner, J.D., Rosenfeld, J.S., Regier, H.A., 1988. The Role of Groundwater in the Impact of
791 Climate Warming on Stream Salmonines. *Fisheries* 13, 2–8.
- 792 Nelms, D.L., Moberg, R.M., 2010. Preliminary Assessment of the Hydrogeology and
793 Groundwater Availability in the Metamorphic and Siliciclastic Fractured-Rock Aquifer
794 Systems of Warren County, Virginia. *U.S. Geol. Surv. Investig. Rep.* 2010–5190.
- 795 O’Sullivan, A.M., Devito, K.J., Ogilvie, J., Linnansaari, T., Pronk, T., Allard, S., Curry, R.A.,
796 2020. Effects of Topographic Resolution and Geologic Setting on Spatial Statistical River
797 Temperature Models. *Water Resour. Res.* 56, 1–23. <https://doi.org/10.1029/2020WR028122>
- 798 Odom, W.E., Doctor, D.H., Burke, C.E., Cox, C.L., 2021. Using high-resolution LiDAR and
799 deep learning models to generate minimum thickness maps of surficial sediments, in:
800 Geological Society of America Abstracts with Programs, v. 53. Portland, OR.
801 <https://doi.org/10.1130/abs/2021AM-367681>
- 802 Payn, R.A., Gooseff, M.N., McGlynn, B.L., Bencala, K.E., Wondzell, S.M., 2009. Channel
803 water balance and exchange with subsurface flow along a mountain headwater stream in
804 Montana, United States. *Water Resour. Res.* 45. <https://doi.org/10.1029/2008wr007644>
- 806 Pelletier, J.D., Broxton, P.D., Hazenberg, P., Zeng, X., Troch, P.A., Niu, G.-Y., Williams, Z.,
807 Brunke, M.A., Gochis, D., 2016. A gridded global data set of soil, intact regolith, and
808 sedimentary deposit thicknesses for regional and global land surface modeling. *J. Adv.
809 Model. Earth Syst.* 8. <https://doi.org/10.1002/2015MS000526>
- 810 Plummer, L.N., Busenberg, E., Bohlke, J.K., Nelms, D.L., Michel, R.L., Schlosser, P., 2001.
811 Groundwater residence times in Shenandoah National Park, Blue Ridge Mountains,
812 Virginia, USA: a multi-tracer approach. *Chem. Geol.* 179, 93–111.
- 813 Rolls, R.J., Leigh, C., Sheldon, F., 2012. Mechanistic effects of low-flow hydrology on riverine
814 ecosystems: Ecological principles and consequences of alteration. *Freshw. Sci.* 31, 1163–
815 1186. <https://doi.org/10.1899/12-002.1>
- 816 Shangguan, W., Hengl, T., Mendes de Jesus, J., Yuan, H., Dai, Y., 2017. Mapping the global
817 depth to bedrock for land surface modeling. *J. Adv. Model. Earth Syst.* 9, 65–88.
818 <https://doi.org/10.1002/2016MS000686>
- 819 Sidle, R.C., Tsuboyama, Y., Noguchi, S., Hosoda, I., Fujieda, M., Shimizu, T., 2000. Stormflow
820 generation in steep forested headwaters: A linked hydrogeomorphic paradigm. *Hydrol.
821 Process.* 14, 369–385. [https://doi.org/10.1002/\(SICI\)1099-1085\(20000228\)14:3<369::AID-
822 HYP943>3.0.CO;2-P](https://doi.org/10.1002/(SICI)1099-1085(20000228)14:3<369::AID-HYP943>3.0.CO;2-P)
- 823 Singha, K., Navarre-Sitchler, A., 2021. The importance of groundwater in critical zone science.
824 *Groundwater* 1–8. <https://doi.org/10.1111/gwat.13143>
- 825 Snyder, C.D., Hitt, N.P., Johnson, Z.C., 2017. Air-water temperature data for the study of



- 826 groundwater influence on stream thermal regimes in Shenandoah National Park, Virginia:
827 U.S. Geological Survey data release. <https://doi.org/https://doi.org/10.5066/F7B56H72>
- 828 Snyder, C.D., Hitt, N.P., Young, J.A., 2015. Accounting for groundwater in stream fish thermal
829 habitat responses to climate change. *Ecol. Appl.* 00, 281–304.
- 830 Snyder, C.D., Webb, J.R., Young, J.A., Johnson, Z.B., Jewell, S., Survey, U.S.G., 2013.
831 Significance of Headwater Streams and Perennial Springs in Ecological Monitoring in
832 Shenandoah National Park. Open-File Rep. 2013–1178 46.
- 833 Southworth, S., Aleinikoff, J.N., Bailey, C.M., Burton, W.C., Crider, E.A., Hackley, P.C.,
834 Smoot, J.P., Tollo, R.P., 2009. Geologic Map of the Shenandoah National Park Region,
835 Virginia. US Geol. Surv. Open-File Rep. 2009–1153 1.
- 836 Stonestrom, D.A., Constantz, J., 2003. Heat as a Tool for Studying the Movement of Ground
837 Water Near Streams. U.S. Geol. Surv. Circ., 1260, 1–6. 96.
- 838 Sullivan, C., Vokoun, J., Helton, A., Briggs, M.A., Kurylyk, B., 2021. An ecohydrological
839 typology for thermal refuges in streams and rivers. *Ecohydrology*.
840 <https://doi.org/10.1002/eco.2295>
- 841 Tiwari, T., Buffam, I., Sponseller, R.A., Laudon, H., 2017. Inferring scale-dependent processes
842 influencing stream water biogeochemistry from headwater to sea. *Limnol. Oceanogr.* 62,
843 S58–S70. <https://doi.org/10.1002/lno.10738>
- 844 Tonina, D., Buffington, J.M., 2009. Hyporheic Exchange in Mountain Rivers I: Mechanics and
845 Environmental Effects. *Geogr. Compass* 3, 1063–1086. <https://doi.org/10.1111/j.1749-8198.2009.00226.x>
- 847 Tran, H., Zhang, J., Cohard, J.M., Condon, L.E., Maxwell, R.M., 2020. Simulating
848 Groundwater-Streamflow Connections in the Upper Colorado River Basin. *Groundwater*
849 58, 392–405. <https://doi.org/10.1111/gwat.13000>
- 850 Ward, A.S., Schmadel, N.M., Wondzell, S.M., 2018. Simulation of dynamic expansion,
851 contraction, and connectivity in a mountain stream network. *Adv. Water Resour.* 114, 64–
852 82. <https://doi.org/10.1016/j.advwatres.2018.01.018>
- 853 Ward, A.S., Wondzell, S.M., Schmadel, N.M., Herzog, S.P., 2020. Climate Change Causes River
854 Network Contraction and Disconnection in the H.J. Andrews Experimental Forest, Oregon,
855 USA. *Front. Water* 2, 1–10. <https://doi.org/10.3389/frwa.2020.00007>
- 856 Weekes, A.A., Torgersen, C.E., Montgomery, D.R., Woodward, A., Bolton, S.M., 2015.
857 Hydrologic response to valley-scale structure in alpine headwaters. *Hydrol. Process.* 29,
858 356–372. <https://doi.org/10.1002/hyp.10141>
- 859 Wehrly, K., Wang, L., Mitro, M., 2007. Field-based estimates of thermal tolerance limits for
860 trout: incorporating exposure time and temperature fluctuation. *Trans. Am. Fish. Soc.* 136,
861 365–374.
- 862 Winter, T.C., Harvey, J.W., Franke, O.L., Alley, W.M., 1998. Ground water and surface water: a
863 single resource. U. S. Geol. Surv. Circ. 1139 79.
- 864 Wohl, E., 2017. Connectivity in rivers. *Prog. Phys. Geogr.* 41, 345–362.

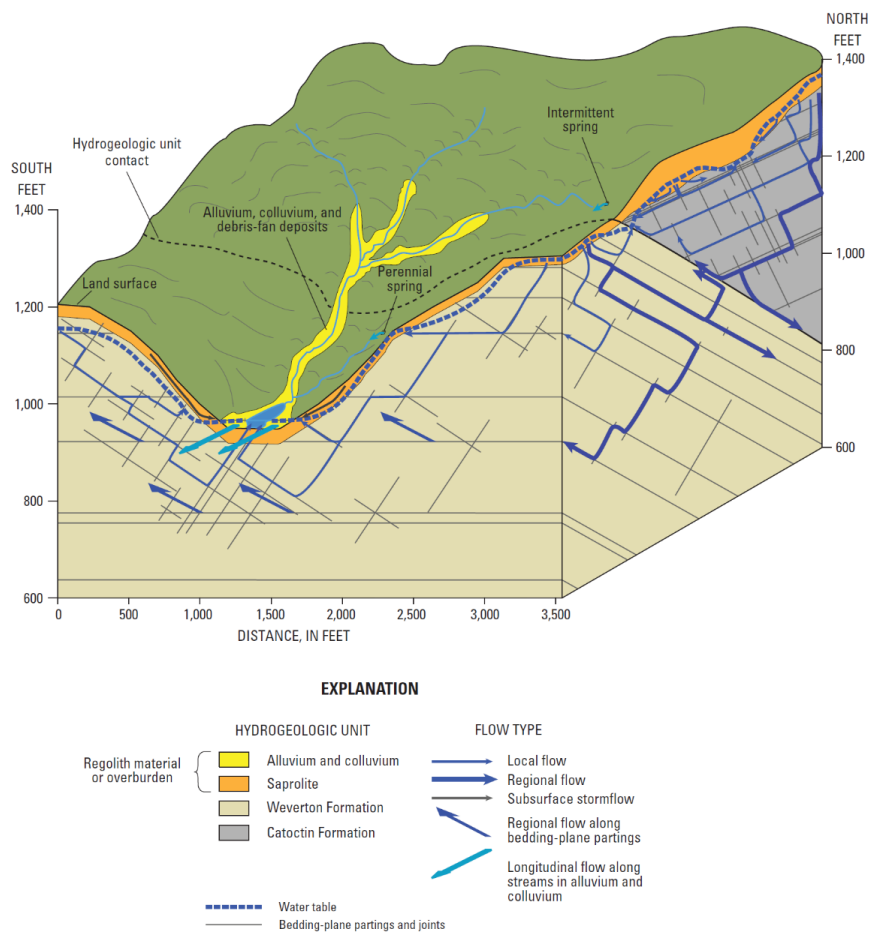


- 865 <https://doi.org/10.1177/0309133317714972>
- 866 Wu, L., Gomez-Velez, J.D., Krause, S., Singh, T., Wörman, A., Lewandowski, J., 2020. Impact
867 of Flow Alteration and Temperature Variability on Hyporheic Exchange. *Water Resour.*
868 *Res.* 56. <https://doi.org/10.1029/2019WR026225>
- 869 Yanamaka, H., Takemura, M., Ishida, H., Niwa, M., 1994. Characteristics of long-period
870 microtremors and their applicability in exploration of deep sedimentary layers. *Bull. Seism.*
871 *Soc. Am.* 84, 1831–1841.
- 872 Zimmer, M.A., McGlynn, B.L., 2017. Bidirectional stream–groundwater flow in response to
873 ephemeral and intermittent streamflow and groundwater seasonality. *Hydrol. Process.* 31,
874 3871–3880. <https://doi.org/10.1002/hyp.11301>



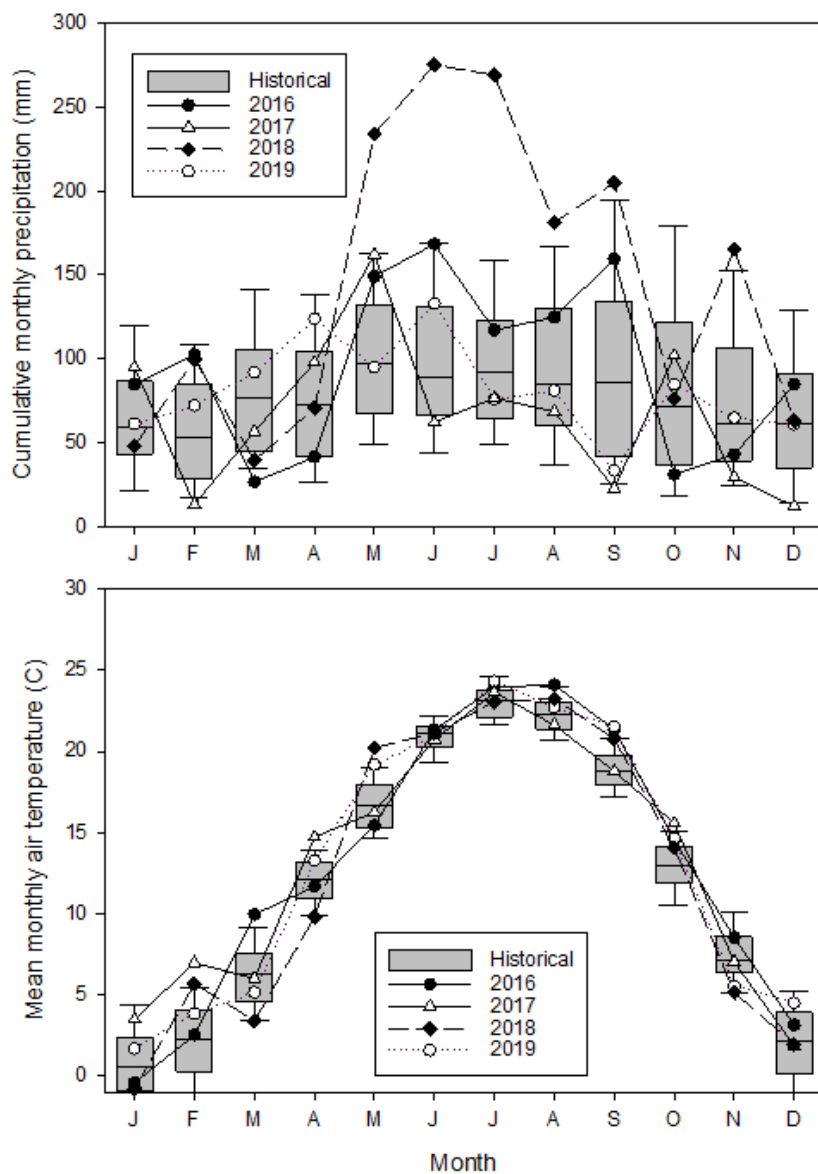
875

876 **Appendix A**



878 Figure A1. The headwater streams of Shenandoah National Park, Virginia, USA are expected to
 879 flow over coarse alluvium and colluvium and have connectivity to shallow hillslope groundwater
 880 and underflow, but reduced connectivity to deeper bedrock groundwater (Modified Figure 26 in
 881 (Nelms and Moberg, 2010) *U.S. Geol. Surv. Investigations Rep.* 2010–5190.

882

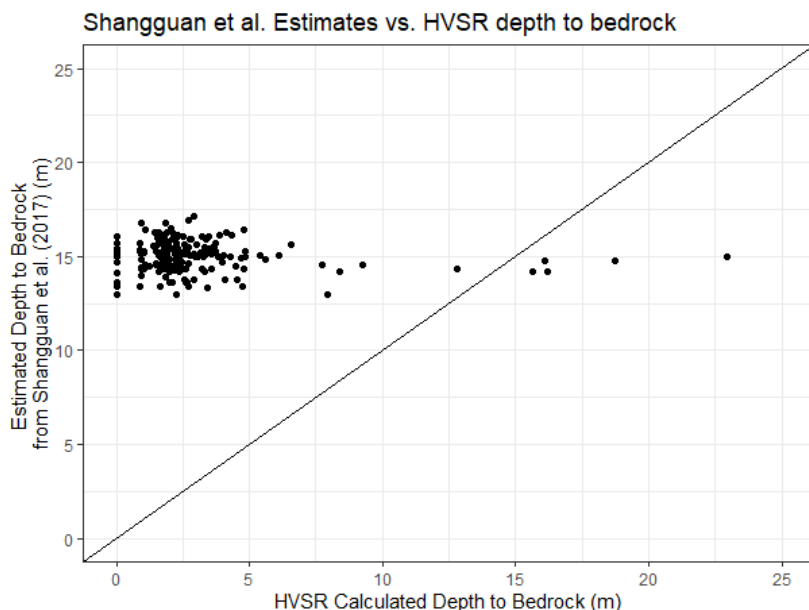


884 Figure A2. Monthly precipitation and air temperature data derived from the Luray weather
885 station (GHCND:USC00445096) located within Shenandoah National Park. Box plots show the
886 distribution of values for the period of record (1942-2020) with the limits of the box containing
887 50% of the values, whiskers containing 90% of the values, and solid line in boxes depicting the
888 median value. The lines represent values for the four primary study years.

889



891 Figure A3. Images from the same vantage point along Paine Run during a) high and b) low flow
892 times, the latter showing channel dewatering associated with a deposit of coarse alluvium across
893 the channel.



895 Figure A4: Comparison between bedrock depth modeled for the globe by Shangguan et al.,
 896 (2017) at a 250m resolution and the HVSr-calculated depths to bedrock in this study.

897

898 **Appendix B**

899 Table B1. Summer stream temperature metrics for each study subwatershed determined from the
 900 data set of Snyder et al. (2017), doi.org/10.5066/F7B56H72.

Subwatershed	SiteID	Easting	Northing	Downstream Distance (m)	summer mean (°C)	7-d min (°C)	7-d max (°C)	Stddev (°C)
Hughes	HUR1MP	730038	4276000	242.50	13.43	11.50	16.07	0.98
Hughes	HUR3LCP	731058	4275970	1634.44	15.73	13.23	18.21	1.24
Hughes	HUR5LCP	732278	4275850	3308.93	16.21	13.48	18.62	1.24
Hughes	HUR6MP	733348	4275060	5163.46	16.39	13.86	17.95	1.13
Hughes	HUR12MP	733698	4274880	5620.73	16.79	14.09	18.34	1.24
Hughes	HUR8LCP	733988	4274619	6219.50	18.80	15.19	21.49	1.57
Hughes	HUR9LCP	733968	4274529	6284.35	17.59	14.49	20.09	1.34
Hughes	HUR10MP	734928	4273520	8187.04	18.05	15.01	20.05	1.40
Hughes	HUR13MP	735258	4273330	8667.16	18.68	15.15	21.18	1.62
Hazel	HZR1MP	735158	4278560	707.45	16.80	13.26	19.75	1.46
Hazel	HZR3LCP	735498	4278760	1190.18	16.74	13.08	19.41	1.50
Hazel	HZR11MP	736378	4279640	2951.89	18.16	15.34	20.32	1.52



Hazel	HZR5MP	736638	4279790	3331.66	17.59	13.59	20.62	1.67
Hazel	HZR6MP	737498	4279059	5095.01	18.16	14.03	21.40	1.74
Hazel	HZR7MP	738048	4277990	6820.13	18.48	14.50	21.77	1.72
Hazel	HZR9MP	738368	4277620	7478.33	18.50	14.74	21.72	1.63
Jeremy's	JR1MP	734618	4293430	102.97	15.48	12.42	18.74	1.41
Jeremy's	JR2MP	733908	4293130	1268.08	16.49	13.38	19.42	1.38
Jeremy's	JR4MP	732498	4292250	3699.53	16.84	14.23	18.22	1.11
Jeremy's	JR5MP	731778	4290670	5961.22	17.54	14.15	20.24	1.43
Jeremy's	JR13MP	731498	4289490	7506.87	18.16	14.57	21.28	1.67
Jeremy's	JR7MP	730068	4288080	10327.83	18.76	16.79	21.07	1.10
Jeremy's	JR9LCP	729888	4288080	10539.49	17.78	15.33	20.01	1.04
Jeremy's	JR12MP	728758	4288080	12030.09	18.61	14.46	22.08	1.73
Jeremy's	JR10MP	727758	4288440	13376.47	19.55	14.93	23.55	1.98
Meadow	MR0MP	695318	4228150	0.00	14.16	12.01	15.57	1.07
Meadow	MR1MP	695038	4227980	217.46	16.82	13.82	18.39	1.28
Meadow	MR2MP	694678	4227520	979.43	17.11	13.71	18.78	1.48
Meadow	MR9MP	693488	4227270	2757.87	18.10	15.34	19.71	1.31
Meadow	MR4LCP	693428	4227240	2854.69	17.01	13.92	19.02	1.44
Meadow	MR8MP	693078	4226450	4036.50	17.53	14.32	19.48	1.35
Meadow	MR6LCP	692918	4226170	4446.20	17.08	14.34	19.32	1.29
Meadow	MR7MP	691738	4225700	6209.68	18.37	15.33	20.44	1.44
Paine	PAR1MP	696938	4232031	249.71	16.86	13.96	18.72	1.36
Paine	PARB1	696718	4231390	1115.08	17.20	14.81	18.70	1.15
Paine	PAR2MP	696468	4231210	1542.16	17.15	15.22	18.61	1.03
Paine	PAR3MP	695685	4230400	3169.18	17.48	14.93	19.28	1.15
Paine	PAR5LCP	695369	4230040	3861.10	17.87	15.01	19.53	1.32
Paine	PAR9MP	694568	4229850	5016.00	18.04	15.43	19.60	1.12
Paine	PAR6MP	694218	4229700	5563.29	18.39	14.86	20.32	1.52
Paine	PAR10MP	694068	4229730	5829.23	18.62	14.71	20.50	1.65
Paine	PARB2	693248	4230140	7055.48	18.60	14.54	20.57	1.67
Paine	PAR8MP	693137	4230180	7122.47	18.84	14.50	20.91	1.97
Piney	PIR1MP	736308	4292604	402.61	15.67	12.24	19.16	1.65
Piney	PIR3LCP	736218	4291980	1199.93	16.43	12.76	19.78	1.65
Piney	PIR4MP	735598	4291160	2480.47	16.55	13.24	19.65	1.51
Piney	PIR5MP	735458	4290050	3955.00	16.82	13.62	19.97	1.48
Piney	PIR6MP	736408	4289180	5862.79	17.74	15.87	20.49	1.15
Piney	PIR7MP	736748	4288300	7115.97	17.40	15.07	20.22	1.17
Piney	PIR8MP	737538	4287390	8756.79	17.88	14.63	20.55	1.39
Staunton	SR1MP	725248	4260810	477.07	14.64	11.96	17.33	1.32
Staunton	SR2MP	725908	4260450	1412.13	15.16	12.34	18.15	1.44
Staunton	SR5MP	726948	4259890	2907.57	15.92	13.03	19.08	1.51



Staunton	SR6MP	728018	4259921	4398.87	16.45	13.48	19.38	1.48
Staunton	SR10MP	728598	4259660	5220.08	17.12	13.88	19.84	1.48
Staunton	SR7MP	728718	4259390	5627.21	17.09	13.99	20.02	1.52
Staunton	SR9MP	729448	4258420	7519.72	17.41	14.57	19.88	1.33
White Oak	WOC1MP	728788	4273701	469.03	13.51	11.85	14.91	0.74
White Oak	WOC3MP	728998	4273160	1237.37	15.43	12.67	17.90	1.29
White Oak	WOC4MP	729268	4272400	2307.96	15.71	12.52	18.58	1.48
White Oak	WOC5MP	730288	4271180	4428.05	17.90	14.23	21.16	1.77
White Oak	WOC7LCP	730758	4270690	5302.94	18.69	15.02	22.07	1.79
White Oak	WOC8MP	730948	4269150	7356.87	18.29	15.88	19.78	1.07
White Oak	WOCB	731018	4269110	7448.09	18.71	16.04	21.18	1.28

901

902

903

904

905

906

907

908

909

910

911